PHYSICAL REVIEW E **106**, 014120 (2022)

Role of extended coupling in bidirectional transport system

Tamizhazhagan S and Atul Kumar Verma[*]
Department of Mathematics, National Institute of Technology, Tiruchirappalli 620 015, Tamilnadu, India

(Received 17 February 2022; revised 1 June 2022; accepted 23 June 2022; published 18 July 2022)

Motivated by vehicular traffic phenomena, we study a bidirectional two-lane open totally asymmetric simple exclusion process with extended symmetric coupling conditions in the presence of Langmuir kinetics. The phase diagrams and density profiles are calculated utilizing mean-field theory for different lane-changing rates and are found to be in a good match with Monte Carlo simulation results. It has been observed that the qualitative topology of phase diagrams depends on the lane-switching rate significantly, resulting in nonmonotonic variations in the number of steady-state phases. The proposed model provides various mixed phases leading to bulk induced phase transitions. The interplay between bidirectional movement, extended coupling conditions, and Langmuir kinetics produces unusual phenomena, including a back-and-forth phase transition and partial phase division of the shock region for comparatively smaller values of the lane-changing rate. Moreover, we analyze the shock dynamics and calculate critical values for the lane-changing rate at which the phases appear or disappear.

DOI: 10.1103/PhysRevE.106.014120

I. INTRODUCTION

Many natural and artificial transport systems develop into a nonequilibrium state and reveal various complex features under an interrupted supply of internal or external energy. In recent years this category of systems has been extensively explored due to its rich presence in biology, physics, and chemistry, including vehicular traffic, ant trails, protein synthesis, intracellular transports carried out by molecular motors, and gel electrophoresis [1–10]. The totally Asymmetric Simple Exclusion Process (TASEP), a particular case of driven diffusive systems, has been contemplated as a simple stochastic model for investigating different kinds of transport systems. In 1968 MacDonald and Gibbs proposed TASEP to analyze the complex phenomena of the kinetics of biopolymerization [11]. This model contains a one-dimensional lattice where particles move in a unique direction. In TASEP, a particle can enter (leave) the lattice through the first (last) site and hops in bulk with predefined rates following the hard-core exclusion principle. It has been widely used to illustrate the stochastic dynamics of multiparticle systems arising in real life. TASEP mimics not only the transport systems but also explains some of the complicated nonequilibrium features such as phase separation, shock formation, boundary-induced phase transition, and symmetry breaking [12–21].

Since, in various transport processes, a particle can join or leave the bulk of the path, based on this observation, recently researchers have proposed TASEP with the incorporation of Langmuir kinetics (LK) dynamics, where the surrounding particles interact with bulk sites of the lattice [15]. TASEP coupled with LK not only helps in analyzing the transport processes more realistically but also produces various nontrivial features in the phase diagram, including localization of shock for a single channel TASEP as addressed in previous studies [15,22]. In this direction, various studies have been conducted on single-channel TASEP coupled with LK, and it has been reported that additional nonconserving dynamics alter the steady-state properties significantly [14,15,22–24].

Further, in various transport processes particles travel along more than one lane and switch between the lanes. For example, motor proteins can move along parallel microtubules forming a multilane system. Also, a driver can change the vehicle from one lane to another according to the surrounding situation in vehicular traffic. These phenomena have inspired researchers to analyze the nonequilibrium stationary character of the multilane system with symmetric and asymmetric coupling rules [25–33]. Further, to make traffic models more realistic, the steady-state properties of multilane TASEP models associated with and without LK have been studied comprehensively [25,26,33–42]. Moreover, ranging from intracellular to vehicular transport, there are various cases where particles move along two paths in opposite directions resulting in a bidirectional transport system. Researchers have conducted different studies on bidirectional TASEP which produced various nontrivial features [20,21,43–50]. Apart from these studies, very recently, Yamamoto *et al.* have studied a two-lane coupled system with extended LK and modified hopping rules under unidirectional as well as bidirectional movement and showed that interactions between lanes affect the system dynamics significantly [38]. One can follow Refs. [2,42] for more studies on the coupled traffic systems. It is important to note that in most of the past coupled TASEP models, particle lane changing occurs when the forwarding site is occupied on the same lane and the target site on another lane is empty. However, various scenarios are found where lane-changing conditions crucially rely on the occupancy of neighboring sites. For example, in the absence of traffic signal systems, in a two-lane bidirectional road, a driver prefers to switch the lane if there is no vehicle just

---

[*] atulv085@gmail.com

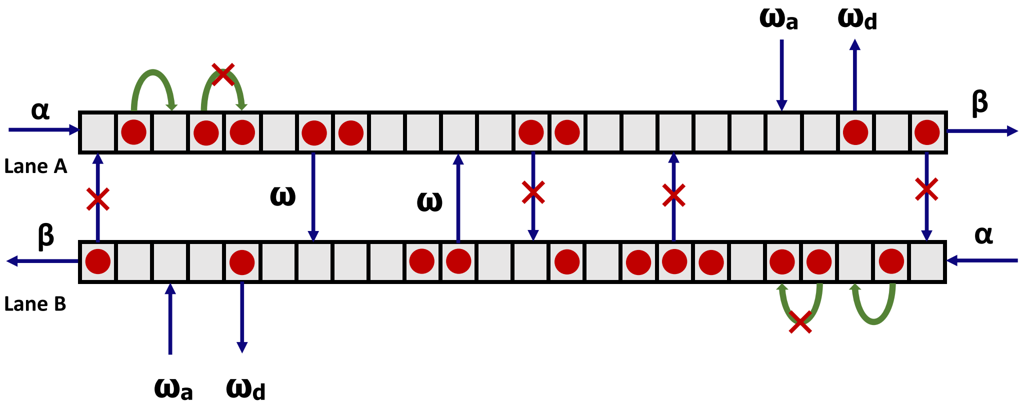

FIG. 1. The model figure of two-lane bidirectional open TASEP with the association of LK and extended coupling rules. The arrows with and without crosses indicate the allowed and forbidden transitions. The parameters α, β, ω_a, ω_d, and ω represent the entry, exit, attachment, detachment, and coupling rates.

behind on the traveling lane and there is a sufficient place available on the opposite road to switch the lane without fear of a collision. Inspired by this example, in this study we introduce a coupling rule (extended coupling) different from the usual one, motivated by the bidirectional vehicular traffic phenomena. As per these coupling rules, the particle lane switching depends on the occupancy of an immediate previous neighboring site on the same lane, the target site, and its following site on another lane. We explore the impact of extended coupling conditions on system dynamics in the presence of bidirectional movement and Langmuir kinetics. To do so, we calculate various steady-state characteristics, including density profiles, phase diagrams, phase transitions, and shock dynamics for the lane-changing rate. We highlight the phase diagram's qualitative and quantitative topological changes emerging due to variations in the lane-changing rate. Note that since this is a first step towards analyzing the influence of extended coupling on system dynamics, we restrict the study to symmetric coupling only, and the more general case of an asymmetric case will be taken up in future studies. Since biological motor proteins can change their lanes without following extended coupling conditions, we discuss a few significant results in Appendix A to mimic this situation and understand the system dynamics in the absence of proposed extended coupling.

We discuss the proposed model in this paper as follows: Sec. II explains the model description, while mean-field equations are presented in Sec. III. Results are discussed in Sec. IV. Finally, we give a summary and conclusions of the problem in Sec. V.

II. MODEL DESCRIPTION

We consider an open system consisting of two parallel one-dimensional lattices, each with L number of sites, denoted by A and B. In lane A (B), particles move from left (right) to the right (left) following the hard-core exclusion principle due to which a site can accommodate at most one particle as shown in Fig. 1. The occupancy state of the site is represented by a binary variable $n_{i,j}$, where $i = 1, 2, \dots, L$ and $j = A, B$. It takes the value 1 or 0 depending on whether the site is occupied or vacant, respectively. At each time step, a site is selected randomly, and random sequential update rules are implemented. Note that the dynamical rules for both lanes are similar except for the opposite movement directions. The subprocesses which govern the system dynamics are as follows:

1. At the entrance site of the lanes: A particle can enter into the vacant first (last) site of lane A (B) with rate α.

2. At the bulk sites of the lanes: If a chosen site (i, j) is empty, a particle can attach to the site with the rate ω_a. If the selected site (i, j) is occupied, the particle first tries to detach from the site with the rate ω_d, and in the case when it fails, it moves to the forward site in the same lane with the unit rate provided the next site is empty. If hopping from site (i, A) $[(i, B)]$ is not possible, then the particle shifts to the corresponding vacant site in another lane (i, B) $[(i, A)]$ with a rate ω provided the sites $(i-1, A)$ $[(i+1, B)]$ and $(i+1, B)$ $[(i-1, A)]$ are empty.

3. At the exit site of the lanes: A particle can exit from lane A (B) with rate β if the last (first) is occupied by a particle.

It is important to note that the above dynamical rules are adopted based on the vehicular traffic phenomenon where drivers prefer to switch the lane only if there is no one immediately behind their vehicle and on the target lane no other vehicle is about to reach the target site to avoid any collision. We hope that the adopted processes will provide better insight into the dynamics of vehicular motion along two parallel roads. The above-mentioned dynamical rules are based on vehicular traffic situations, while the same extended coupling rules are not directly applicable in the case of intracellular transport carried out by motor proteins. Note that, to focus on vehicular traffic, we have not considered the simple coupling, which is also yet to be studied in literature with other adopted dynamical rules. However, to explore the system properties in the absence of proposed extended coupling and to mimic motor proteins' movement, an extension of the presented model is possible on similar lines by removing the extended coupling conditions and keeping only simple coupling rules as discussed in Appendix A. It has been found that the removal of extended coupling conditions reduces the complications of the proposed model and does not affect the system dynamics significantly, which inspired us to ignore them in the further analysis and incorporate them separately to avoid the extra lengthy calculations. Similarly, when the motion of particles is the same in each lane, we retrieve a model studied in the literature with simple coupling [36]. For the sake of completeness and to understand the impact of unidirectional movement on system dynamics, we have presented the proposed model by removing bidirectional movement and incorporating motion in only one direction in both lanes in Appendix B. Therefore, the above considerations make our model more general and realistic compared to the existing models [25–37,39,40] accounting for the coupling between parallel lanes to mimic transport systems.

III. MEAN-FIELD APPROXIMATION

The resulting master equations for the occupancy of bulk sites ($1 < i < L$) in both lanes ($j = A, B$) are described as follows:

$$\begin{aligned}\frac{d\langle n_{i,A}\rangle}{dt} &= \langle n_{i-1,A}(1-n_{i,A})\rangle - \langle n_{i,A}(1-n_{i+1,A})\rangle\\ &\quad + \omega_a\langle(1-n_{i,A})\rangle - \omega_d\langle n_{i,A}\rangle\\ &\quad - \omega\langle n_{i,A}n_{i+1,A}(1-n_{i,B})(1-n_{i+1,B})(1-n_{i-1,A})\rangle\\ &\quad + \omega\langle n_{i,B}n_{i-1,B}(1-n_{i,A})(1-n_{i-1,A})(1-n_{i+1,B})\rangle,\end{aligned} \tag{1}$$

$$\begin{aligned}\frac{d\langle n_{i,B}\rangle}{dt} &= \langle n_{i+1,B}(1-n_{i,B})\rangle - \langle n_{i,B}(1-n_{i-1,B})\rangle\\ &\quad + \omega_a\langle(1-n_{i,B})\rangle - \omega_d\langle n_{i,B}\rangle\\ &\quad + \omega\langle n_{i,A}n_{i+1,A}(1-n_{i,B})(1-n_{i+1,B})(1-n_{i-1,A})\rangle\\ &\quad - \omega\langle n_{i,B}n_{i-1,B}(1-n_{i,A})(1-n_{i-1,A})(1-n_{i+1,B})\rangle,\end{aligned} \tag{2}$$

where $\langle\cdot\rangle$ denotes the statistical average and the right-hand side of the equations represents gain, and loss terms are appearing due to the hopping, LK, and lane-switching transitions.

Similarly, at boundaries ($i = 1, L$), the time evolution of densities can be calculated as follows:

$$\frac{d\langle n_{1,A}\rangle}{dt} = \alpha\langle(1-n_{1,A})\rangle - \langle n_{1,A}(1-n_{2,A})\rangle, \tag{3}$$

$$\frac{d\langle n_{1,B}\rangle}{dt} = \langle n_{2,B}(1-n_{1,B})\rangle - \beta\langle n_{1,B}\rangle, \tag{4}$$

$$\frac{d\langle n_{L,B}\rangle}{dt} = \alpha\langle(1-n_{L,B})\rangle - \langle n_{L,B}(1-n_{L-1,B})\rangle, \tag{5}$$

$$\frac{d\langle n_{L,A}\rangle}{dt} = \langle n_{L-1,A}(1-n_{L,A})\rangle - \beta\langle n_{L,A}\rangle. \tag{6}$$

Using the mean-field approximation method, we can neglect the correlation between the state variables, i.e., $\langle n_{i,j}n_{i+1,j}\rangle = \langle n_{i,j}\rangle\langle n_{i+1,j}\rangle$.

To solve the above-mentioned system of equations, we attain the continuum limit of the model by coarse graining the discrete lattice with lattice constant $\epsilon = \frac{1}{L}$ along with rescaling the space and time variable as $x = \frac{i}{L}$ and $t' = \frac{t}{L}$, respectively. To analyze the competition between bulk and boundary sites dynamics, we rescale the attachment, detachment, and lane-changing rates as $\Omega_a = \omega_a L$, $\Omega_d = \omega_d L$, and $\Omega = \omega L$. Replacing the discrete variables $\langle n_{i,j}\rangle$ by a continuous variable $\rho_{i,j}$, and carrying the terms up to the second order in Taylor's series expansion we get

$$\rho_{i\pm1,j} = \rho_{i,j} \pm \frac{1}{L}\frac{\partial\rho_{i,j}}{\partial x} + \frac{1}{2L}\frac{\partial^2\rho_{i,j}}{\partial x^2} \pm O\left(\frac{1}{L^3}\right). \tag{7}$$

Since both lanes do not have any kind of spatial inhomogeneity, we drop the subscript i, which leads to the average bulk sites densities in both lanes as follows:

$$\begin{aligned}\frac{d\rho_A}{dt'} &= \frac{\epsilon^2}{2}\rho_A''[L+r] - \frac{\epsilon^2}{2}\rho_B''[s] + \epsilon\rho_A'[t] + \epsilon\rho_B'[v]\\ &\quad - \Omega\epsilon^2(\rho_A')^2[\rho_A(1-\rho_B)^2] + \Omega\epsilon^2(\rho_B')^2[\rho_B(1-\rho_A)^2]\\ &\quad + \Omega\epsilon^2\rho_A'\rho_B'[\rho_A(1-\rho_B) - \rho_B(1-\rho_A)]\\ &\quad - \Omega(1-\rho_A)(1-\rho_B)\big[\rho_A^2(1-\rho_B) - \rho_B^2(1-\rho_A)\big]\\ &\quad + \Omega_a(1-\rho_A) - \Omega_d\rho_A,\end{aligned} \tag{8}$$

$$\begin{aligned}\frac{d\rho_B}{dt'} &= -\frac{\epsilon^2}{2}\rho_A''[r] + \frac{\epsilon^2}{2}\rho_B''[L+s] - \epsilon\rho_A'[w] - \epsilon\rho_B'[u]\\ &\quad + \Omega\epsilon^2(\rho_A')^2[\rho_A(1-\rho_B)^2] - \Omega\epsilon^2(\rho_B')^2[\rho_B(1-\rho_A)^2]\\ &\quad - \Omega\epsilon^2\rho_A'\rho_B'[\rho_A(1-\rho_B) - \rho_B(1-\rho_A)]\\ &\quad + \Omega(1-\rho_A)(1-\rho_B)[\rho_A^2(1-\rho_B) - \rho_B^2(1-\rho_A)]\\ &\quad + \Omega_a(1-\rho_B) - \Omega_d\rho_B,\end{aligned} \tag{9}$$

where

$$\begin{aligned}r &= \Omega[\rho_A(2\rho_A-1)(1-\rho_B)^2 - \rho_B^2(1-\rho_A)(1-\rho_B)],\\ s &= \Omega[\rho_B(2\rho_B-1)(1-\rho_A)^2 - \rho_A^2(1-\rho_A)(1-\rho_B)],\\ t &= \Omega[2\rho_A - 1 - \rho_A(1-\rho_B) + \rho_B^2(1-\rho_A)(1-\rho_B)],\\ u &= \Omega[2\rho_B - 1 - \rho_B(1-\rho_A) + \rho_A^2(1-\rho_A)(1-\rho_B)],\\ v &= \Omega[\rho_A^2(1-\rho_A)(1-\rho_B) - \rho_B(1-\rho_A)],\\ w &= \Omega[\rho_B^2(1-\rho_A)(1-\rho_B) - \rho_A(1-\rho_B)].\end{aligned}$$

Similarly, the density evolution of boundary sites of the lanes are characterized as follows:

$$\frac{d\rho_{1,A}}{dt'} = \frac{1}{\epsilon}\alpha(1-\rho_{1,A}) - \frac{1}{\epsilon}\rho_{1,A}(1-\rho_{2,A}), \tag{10}$$

$$\frac{d\rho_{1,B}}{dt'} = \frac{1}{\epsilon}\rho_{2,B}(1-\rho_{1,B}) - \frac{1}{\epsilon}\beta\rho_{1,B}, \tag{11}$$

$$\frac{d\rho_{L,A}}{dt'} = \frac{1}{\epsilon}\rho_{L-1,A}(1-\rho_{L,A}) - \frac{1}{\epsilon}\beta\rho_{L,A}, \tag{12}$$

$$\frac{d\rho_{L,B}}{dt'} = \frac{1}{\epsilon}\alpha(1-\rho_{L,B}) - \frac{1}{\epsilon}\rho_{L,B}(1-\rho_{L-1,B}). \tag{13}$$

To obtain the steady-state solution of the coupled nonlinear system (8)–(13), We utilize the singular perturbation technique, which in the past has successfully explained the complete phase diagrams of single as well as multichannel TASEP with LK [35,36,40,51].

IV. RESULTS AND DISCUSSION

A. Phase diagram

We analyze the steady-state behavior of the proposed system in the presence of LK under the influence of extended

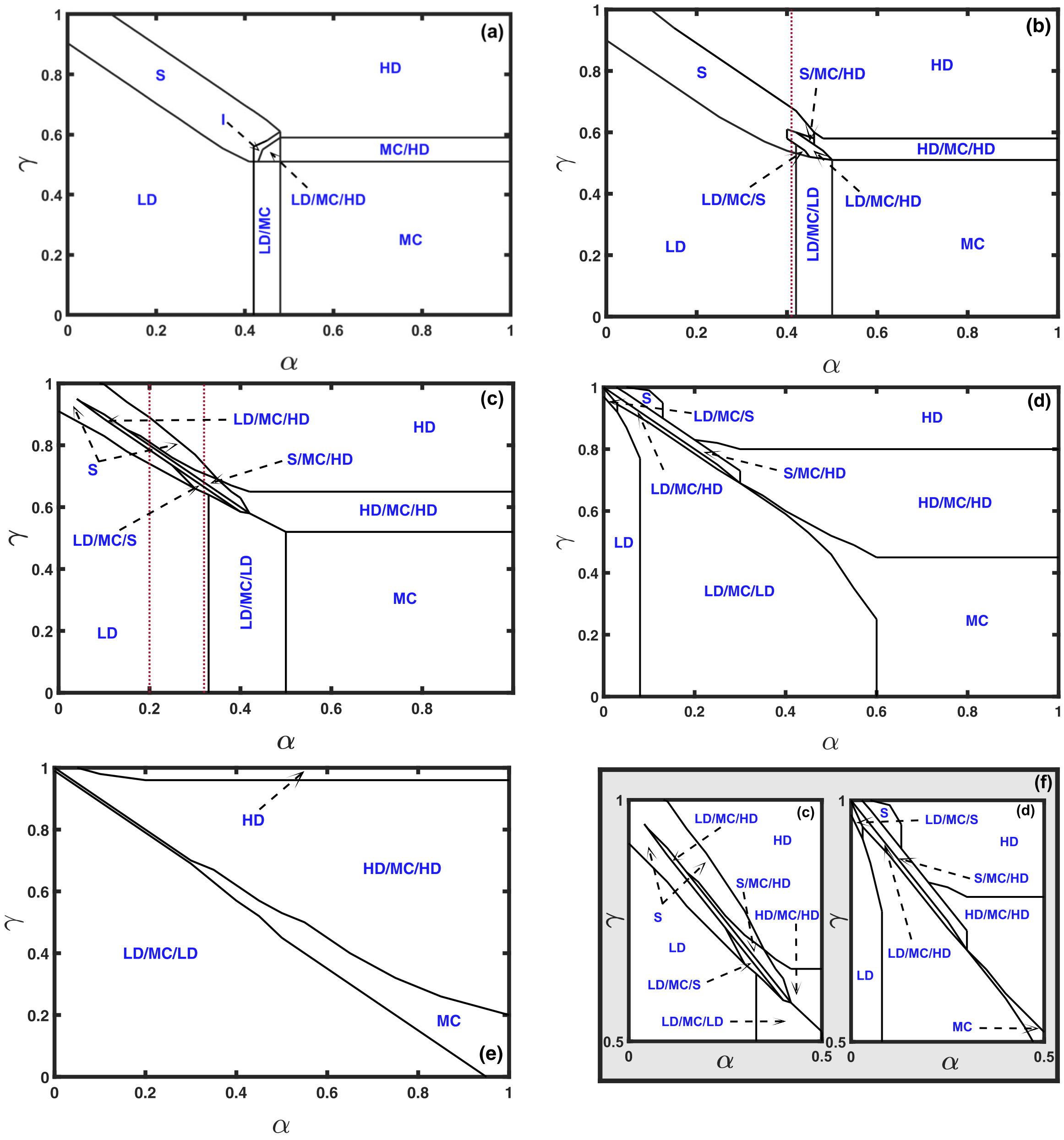

FIG. 2. Phase diagram for (a) $\Omega = 0.1$, (b) $\Omega = 1$, (c) $\Omega = 10$, (d) $\Omega = 100$, (e) $\Omega = 1000$ with $\Omega_a = \Omega_d = 0.1$ and $L = 1000$. (f) Zoomed view of specific region of (c) and (d) to enhance the clarity.

coupling conditions. Note that in the current study, we focus on the special case of $\Omega_a = \Omega_d$ and investigate the role of extended coupling on the steady-state system properties.

For a comprehensive analysis, we calculate phase diagrams for specific values of the lane-changing rate $\Omega \in [0, 1000]$ showing significant topological changes in the controlling parameter space of (α, γ) where $\gamma = 1 - \beta$. In this direction, phase diagrams with respect to the different lane-changing rates are displayed in Fig. 2. In our proposed model, we obtain 12 types of steady-state phases for the various values of coupling rate as shown in the phase diagrams (see Fig. 2). These 12 phases are (LD, LD), (MC, MC), (HD, HD), (S, S), (I, D), (LD/MC, MC/LD), (MC/HD, HD/MC), (LD/MC/LD, LD/MC/LD)(LD/MC/HD, HD/MC/LD), (LD/MC/S, S/MC/LD), (S/MC/HD, HD/MC/S), and (HD/MC/HD, HD/MC/HD) and are named LD (low density) ($\rho < 0.5$), MC (maximal current)($\rho = 0.5$), HD (high density)($\rho > 0.5$), S (shock), and I (D) where the phase I (D) represents the strictly increasing (decreasing) curve from low (high) density to high (low) density portions. Physically, phase I represents that in the initial part of the path there are fewer particles, while concerning space, this number smoothly increases, leading to a crowded region near the path end. The density profile of the form X/Y/Z is called mixed phases, where X, Y, and Z belong to one among the phases of LD, MC, HD, and S. Note that due to the bidirectional symmetric dynamics of the system, the density profile of one lane is the mirror view of another one, so therefore in the phase diagrams,

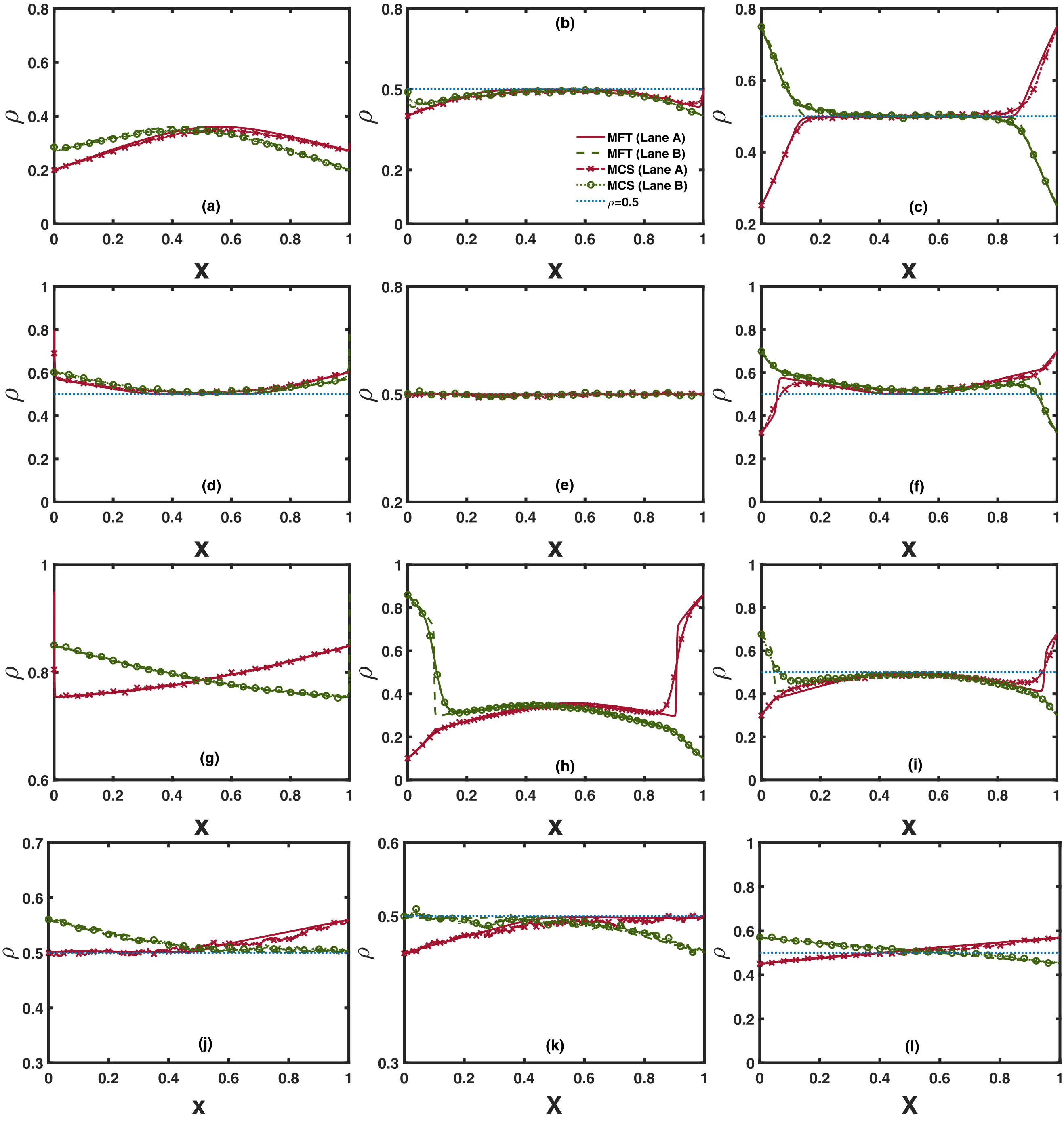

FIG. 3. The density profiles captured for the LK rates $\Omega_a = \Omega_d = 0.1$ and $L = 1000$. For the coupling rate of (1) $\Omega = 10$: (a) LD phase for $\alpha = 0.2$, $\gamma = 0.2$; (b) LD/MC/LD phase for $\alpha = 0.4$, $\gamma = 0.5$; (c) LD/MC/HD phase for $\alpha = 0.25$, $\gamma = 0.75$; (d) HD/MC/HD phase for $\alpha = 0.8$, $\gamma = 0.6$; (e) MC phase for $\alpha = 0.5$, $\gamma = 0.5$; (f) S/MC/HD phase for $\alpha = 0.32$, $\gamma = 0.7$; (g) HD phase for $\alpha = 0.95$, $\gamma = 0.85$; (h) S phase for $\alpha = 0.1$, $\gamma = 0.86$; and (i) LD/MC/S phase for $\alpha = 0.3$, $\gamma = 0.68$. And for that of (2) $\Omega = 0.1$: (j) MC/HD phase for $\alpha = 0.5$, $\gamma = 0.56$; (k) LD/MC phase for $\alpha = 0.45$, $\gamma = 0.5$; and (l) I phase for $\alpha = 0.45$, $\gamma = 0.57$. The solid (dashed) line indicates the mean-field result, and the crossed (circled) curve represents the simulation result of lane A (B).

instead of denoting names of phases for both lanes, without loss of generality, we mention only lane A density profile names throughout the paper and have demonstrated these phases in the form of density profiles in Fig. 3. Phases LD, LD/MC/LD, LD/MC/HD, HD/MC/HD, MC, S/MC/HD, HD, S, LD/MC/S, MC/HD, LD/MC, and I are demonstrated in order in the panels of Fig. 3.

Initially, for a comparatively smaller value of $\Omega = 0.01$ (c_1), we observe eight distinct steady-state phases: LD [Fig. 3(a)], MC [Fig. 3(e)], HD [Fig. 3(g)], S [Fig. 3(h)], I [Fig. 3(l)], LD/MC [Fig. 3(k)], MC/HD [Fig. 3(j)], and LD/MC/HD [Fig. 3(c)] as shown in Fig. 2(a). Note that phase I is a unique phase, which was not reported in past studies of single-channel TASEP with LK, which is a special case

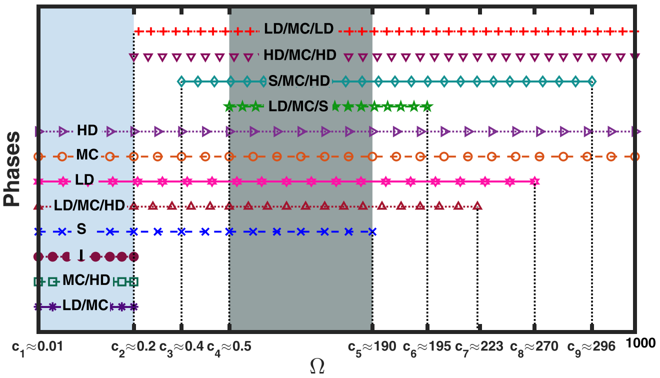

FIG. 4. Observed phase transitions with varied Ω for $L = 1000$. C_i's indicate the critical points beyond which the specific phases either appear or disappear. The colored region indicates the place in which the maximum number of phases occurs commonly.

of our proposed model with $\Omega = 0$ [15,22]. With an increase in Ω, apart from shifting in phase boundaries, no considerable changes are noticed in the phase diagram till $c_2 = 0.2$, at which phases LD/MC, MC/HD, and I disappear while two new phases LD/MC/LD [Fig. 3(b)] and HD/MC/HD [Fig. 3(d)] start emerging as clearly shown in Fig. 2(b). For $\Omega > 0.2$, no significant changes are observed up to $c_3 = 0.4$ at which a new phase S/MC/HD [Fig. 3(f)] starts appearing. If we again enhance Ω from 0.4 to critical $c_4 = 0.5$, a new phase LD/MC/S [Fig. 3(i)] appears. On further enhancement in Ω, the system experiences a unique topological structure in the phase diagram for $\Omega = 1$, which results in an unaccustomed back-and-forth phase transition for some specific and fixed values of α by varying only γ while keeping all other parameters fixed. In particular, one can travel from S to LD/MC/HD to the S phase again (S $\rightarrow$ LD/MC/HD $\rightarrow$ S), unveiling a back-and-forth phase transition as displayed by a dotted line in the phase diagram in Fig. 2(b) [see also Fig. 5(b) below] and defined as follows. If in any phase diagram we start from any phase P_1 which first transits into phase P_2 and then transits into phase P_1 itself ($P_1 \rightarrow P_2 \rightarrow P_1$) with respect to a single parameter by keeping all others parameter fixed, then this type of transition is called a back-and-forth phase transition as in a recent study on TASEP [52] following which we also adopt the same name for such a type of phase transitions as observed in our study. Note that in a few studies in reference to statistical physics, the back-and-forth phase transition is also called a reentrance transition; therefore, we wish to clarify that the back-and-forth transition is similar to the reentrance transition. For $\Omega > 1$, the number of phases remains the same; however, there are significant topological changes in the phase diagram at $\Omega = 10$, leading to a new phenomenon, partial phase fragmentation. More specifically, at this stage, the S phase is divided into two parts by a very narrow region of the LD/MC/HD phase, as visible in Fig. 2(c). In other words, we detect the mixed-phase LD/MC/HD inside the region of the shock phase, which partially divides the shock region into two regions and acts as one of the common phase boundary regions for both mixed phases LD/MC/S and S/MC/HD. It is significant to mention that in past studies of coupled two-lane TASEP with LK as well as without LK in the presence of asymmetric or symmetric coupling conditions, the systems have not captured a back-and-forth transition or partial or complete phase fragmentation to our knowledge. We will discuss these features in more detail below. Also, beyond $\Omega = 10$, apart from shifting in the phase regions, no significant quantitative changes are found in the phase diagram, as shown in the phase diagram for $\Omega = 100$ in Fig. 2(d). For $\Omega > 100$, apart from LD/MC/LD and HD/MC/HD, all other phases start shrinking, leading to the vanishing of the S phase at $c_5 = 190$ followed by the disappearance of the LD/MC/S phase at $c_6 = 195$. If we further increase the value of Ω, we see the exiting of LD/MC/HD, LD, S/MC/HD at critical $c_7 = 223$, $c_8 = 270$, and $c_9 = 296$, respectively. After $\Omega > 296$, there are no quantitative or crucial qualitative changes in the phase diagrams, as also shown in the phase diagram for $\Omega = 1000$, which displays only four phases, LD/MC/LD, HD/MC/HD, HD, and MC, as are clearly visible in Fig. 2(e). Note that in Figs. 2(c) and 2(d), there are a few phases with very narrow regions, making it difficult to read the phase diagrams; therefore, for the sake of clarity, we provide a zoomed view of specific regions of these two-phase diagrams in Fig. 2(f).

To sum up, the above-discussed observations are displayed in Fig. 4 with respect to the lane-changing rate Ω. It is clear from the figure that there exist a total of 12 steady-state phases in the system, including seven mixed phases, out of which most of the phases are not reported in coupled two-lane TASEP models without an extended coupling rule [16,25,33,36,41]. The complexity of the phase diagram differs nonmonotonically with growth in Ω, as initially there are only eight phases in (c_1, c_2), which is reduced to seven in (c_2, c_3), diminishing the complexity in the system. But with the increase in $\Omega \in (c_3, c_4)$, the number of phases again starts increasing from seven to eight and later results in nine phases, which remains a maximum number of steady-state phases for (c_4, c_5). After c_5 when the magnitude of the coupling rate from $\Omega = 190$ is expanding, exactly one phase disappears whenever the value of Ω crosses the critical points. It is observed that, while Ω crosses the critical values c_5, c_6, c_7, c_8, and c_9 explicitly one phase vanishes correspondingly S, LD/MC/S, LD/MC/HD, LD, and S/MC/HD. Therefore beyond c_5, the number of phases continuously decreases with an increase in Ω due to which we notice only four phases for $\Omega = 1000$, resulting in a comparatively simpler phase diagram. Therefore, the system experiences the complexity only for $0 < \Omega < 190$ beyond which the increase in lane-changing rate does not produce any significant outcomes apart from the disappearance of phases, which leads to shifts in the phase boundaries.

The above inspection reveals that extended coupling impacts the system dynamics significantly, as even for minimal values of Ω, we observe eight distinct steady-state phases, including a few mixed phases with various unique properties.

B. Density profiles and phase transitions

The theoretical results calculated using the continuum mean-field theory are validated by performing Monte Carlo simulations (MCSs) for the lattice size $L = 1000$. The simulations are executed for 10^{10} time steps and, the first 5% of the

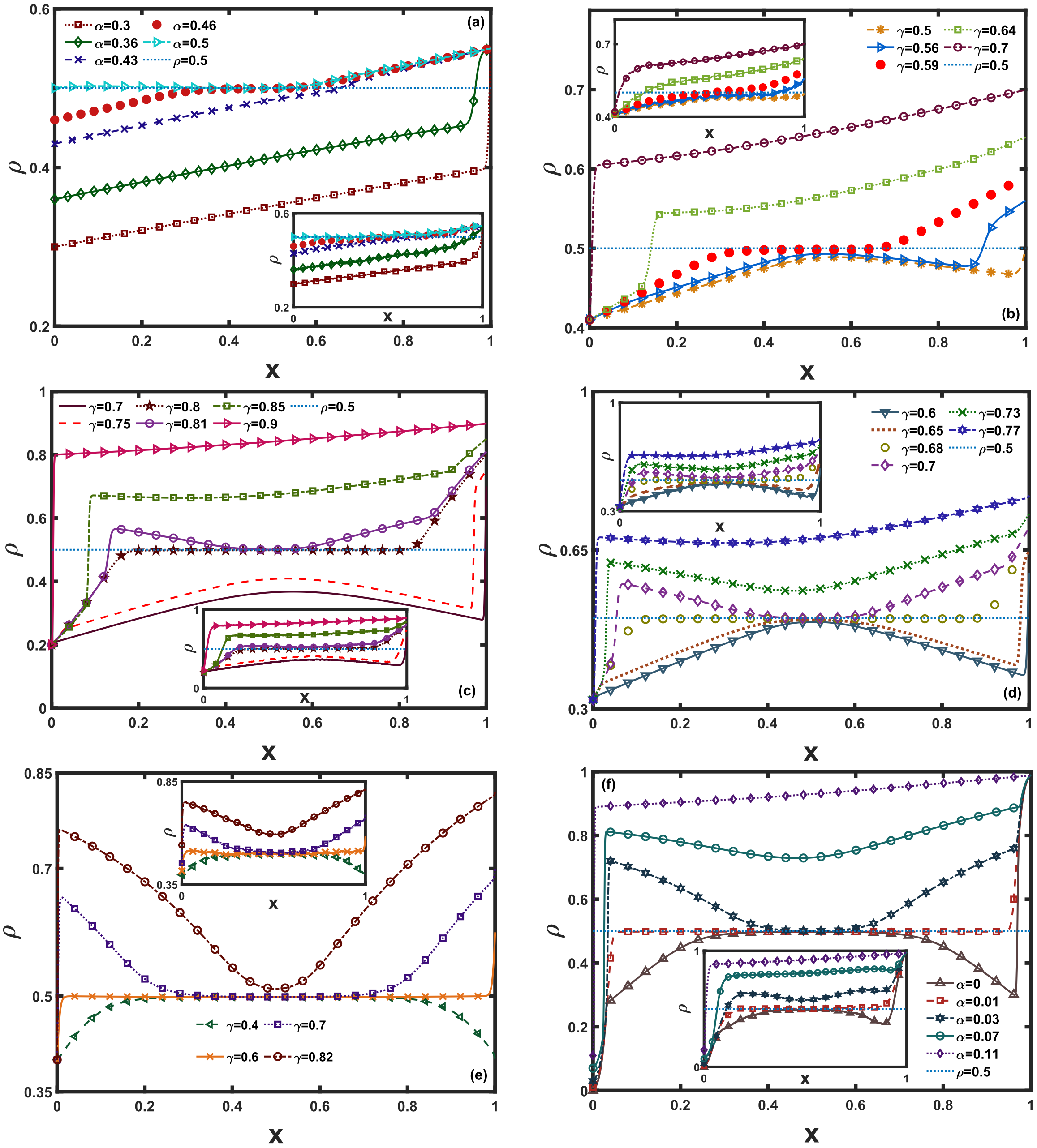

FIG. 5. Phase transitions in lane A from (a) LD → S → I → LD/MC/HD → MC/HD for $\gamma = 0.55$ and $\Omega = 0.1$. (b) LD → S → LD/MC/HD → S → HD for $\alpha = 0.41$ and $\Omega = 1$. (c) LD → LD/MC/S → LD/MC/HD → S/MC/HD → S → HD for $\alpha = 0.32$, $\Omega = 10$. (d) LD → S → LD/MC/HD → S/MC/HD → S → HD with respect to $\alpha = 0.2$, $\Omega = 10$, and different values of γ. (e) LD/MC/LD → MC → HD/MC/HD → HD for $\alpha = 0.4$ with various values of γ and $\Omega = 100$. (f) LD/MC/S → LD/MC/HD → S/MC/HD → S → HD for $\gamma = 0.99$, $\Omega = 100$ with various rates of α and $L = 1000$. The insets indicate the corresponding Monte Carlo simulation results.

time steps are neglected to attain the steady state. The average density in both lanes is calculated by taking the time average over an interval of $10L$. The phase boundaries are computed within an estimated inaccuracy of less than 1%.

In Fig. 3 we have provided all 12 existing stationary phases of our system using mean-field theory and their validation through MCSs. From the figure, it is seen that our theoretical outcomes have good agreement with the simulation results. It is important to note that phases LD/MC/S, S/MC/HD, HD/MC/HD, and LD/MC/LD were not reported in past studies on single-lane TASEP-LK or two-lane coupled TASEP-LK models, which are the special cases of our system [15,22,35,36], which exhibits the significant impact of the extended coupling conditions adopted in our model. It is important to note that in Fig. 3(a), which illustrates the LD phase, we observe a bump indicating a particle accumulation at the center of the lanes, which can be explained as follows. Here entry rate α and exit rate β are 0.2 and 0.8, respectively. From the initial to middle part of the lattice, the density starts increasing due to the slow injection rate. However, once a particle accumulates due to the high exit rate, density starts decreasing concerning space, leading to a bump around the center of the lattice. Further, due to various mixed phases and the crucial role of adopted coupling scenarios, the proposed model displays various interesting steady-state features that can be visualized in terms of phase transitions. In this direction, Fig. 5 shows various nontrivial phase transitions between different phases. The transition from LD to MC/HD with respect to α through phases S, I, LD/MC/HD for $\Omega = 0.1$ with fixed $\gamma = 0.55$ is presented in Fig. 5(a). For $\Omega = 1$, the shape of the phase diagram becomes peculiar, which leads to a unique type of back-and-forth phase transition for some particular and fixed values of the entry rate α by varying only the removal rate β while keeping the remaining parameters fixed. In particular, one can move from S to LD/MC/HD and again to S phase exhibiting a back-and-forth phase transition (S → LD/MC/HD → S) as displayed by a dotted line in the phase diagram shown in Fig. 2(b). For sake of completeness, we show the complete phase transitions LD → S → LD/MC/HD → S → HD for $\alpha = 0.41$. Here S → LD/MC/HD → S is a back-and-forth phase transition. Further, with increased $\Omega = 10$, the phase diagrams become comparatively more complex and strange, which not only shows back-and-forth phase transitions but also partially divides the shock region by other phases which clearly can be observed through the two different phase transitions LD → LD/MC/S → LD/MC/HD → S/MC/HD → S → HD for $\alpha = 0.32$ and LD → S → LD/MC/HD → S/MC/HD → S → HD for $\alpha = 0.2$ as as shown in Figs. 5(c) and 5(d) [see the dotted lines in Fig. 2(c)]. Note that since these transitions take place in bulk only, therefore, they can be referred to as bulk-induced phase transitions. Moreover, it is significant to mention that such types of bulk-induced back-and-forth transitions have not been reported in past studies on single or multilane lane standard TASEP models to our knowledge. Similarly for $\Omega = 100$, there are various bulk induced phase transitions LD/MC/LD → MC → HD/MC/HD → HD for $\alpha = 0.4$ and LD/MC/S → LD/MC/HD → S/MC/HD → S → HD for $\gamma = 0.99$ for the remaining fixed parameters as displayed in Figs. 5(e) and 5(f).

C. Finite-size effect and shock dynamics

Here we inspect the indistinguishable characteristics of shock in the proposed two-lane system. The influence of the system size on the shock profile has also been scrutinized. It is clear from Fig. 6(a) that the vertical sharpness of the profile increases when the lattice size increases, proving that there is no finite-size effect. In the same way, we have verified and observed that the other mixed phases, including those shown in Figs. 3(c), 3(d), 3(f), and 3(i), do not change concerning lattice length, indicating the absence of a finite-size effect as shown in Figs. 6(b)–6(e). Due to the absence of a finite-size effect, the system size does not affect any of the discussed properties of the system. The distinctive aspect of our system is the appearance of back-and-forth transitions of the shock phase, which motivates us to investigate the shock dynamics in terms of its position. In Fig. 7(a) we have shown the shock position of lane A with respect to γ for fixed values of $\alpha = 0.41$ and $\Omega = 1$. Initially, for $\gamma = 0.4$, the system is in the LD phase with a shock position near 1 as a boundary layer which starts shifting from right to left with an increase in γ. On increasing the value of γ from 0.48, the LD phase transits into the shock phase, where the shock profile starts shifting from the right to the left direction resulting in a reduction in the shock position until γ reaches point 0.58. With further increasing γ, the shock phase converts into the mixed-phase LD/MC/HD, which leads to the shock position as zero. For a small range of γ, the system remains in LD/MC/HD, which again transits into the shock phase at $\gamma = 0.6$. Further increasing the value of γ, the position of the shock profile starts decreasing until it reaches the value $\gamma = 0.7$, at which this phase converts into a high-density phase. Beyond all values of γ from 0.7, the HD phase remains so that the shock position is zero. Therefore, we can visualize how the shock phase displays a back-and-forth transition using the shock position by varying only γ. Similarly, we exhibit one more shock position profile in Fig. 7(b) for $\alpha = 0.2$ and $\Omega = 100$ to prove that the valuable feature of the back-and-forth transition persists even for $\Omega = 10$. From Fig. 7 it is clear that the shock position changes nonmonotonically due to the back-and-forth effect. Physically, the existence of the back-and-forth transition signifies that there is a small optimal range for collaboratively higher values of γ for a fixed α in which the system remains in nonshock phases; otherwise the system experiences a shock which represents a traffic jam and is not desired for smooth transportation (Fig. 7). Mathematically, the bidirectional movement (boundary conditions), Langmuir kinetics, and coupling terms in mean-field equations lead to back-and-forth phase transitions. The absence of any of these processes results in this feature's disappearance.

V. CONCLUSION

In this work, motivated by the traffic flow problems, we have analyzed a two-lane bidirectional TASEP model with extended symmetric coupling conditions in which vehicles represented by particles switch the paths depicted as lanes depending on the occupation of neighboring sites in the same as well as in the opposite lane with Langmuir kinetics. Extensively performed Monte Carlo simulations confirm the theoretical results calculated using mean-field theory. To scrutinize the impact of adopted coupling conditions on system properties, various crucial steady-state characteristics such as phase diagrams, density profiles, and phase transitions are computed on the grounds of mean-field approximations. The influence of the coupling rate on the phase diagram is also investigated extensively. The study reports 12 stationary phases, out of which eight phases exhibit mixed behavior, and phases including I, LD/MC/S, S/MC/HD, HD/MC/HD, and LD/MC/LD have not been reported in past studies on single or coupled TASEP models. Since *S* and *HD* lead to a different type of traffic jam resulting in undesirable wastage of time and fuel, therefore, except LD/MC/LD, other mixed phases are not suitable for smooth transportation. The investigation revealed that the extended coupling conditions affect the system dynamics significantly since the same is producing various nontrivial features even for comparatively smaller values of lane-changing rates in the system, which later persist for its higher value. As we enhance the lane-changing rate, crucial topological changes are noticed in the phase diagram qualitatively and quantitatively due to the appearance

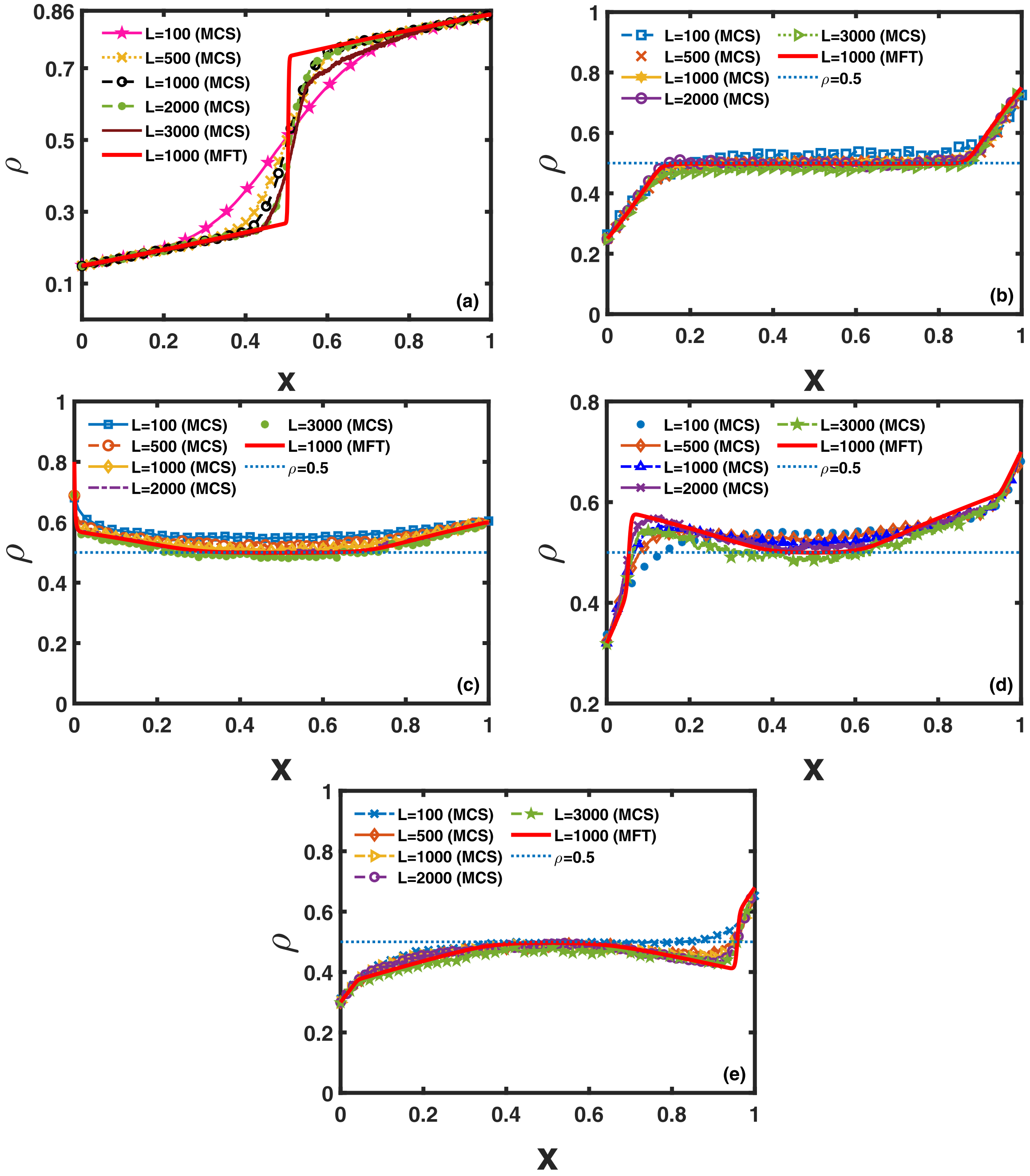

FIG. 6. Finite-size effect on (a) shock phase for $\alpha = 0.15$, $\gamma = 0.85$, and $\Omega = 1$; (b) LD/MC/HD phase for $\alpha = 0.25$, $\gamma = 0.75$, and $\Omega = 10$; (c) HD/MC/HD phase for $\alpha = 0.8$, $\gamma = 0.6$, and $\Omega = 10$; (d) S/MC/HD phase for $\alpha = 0.32$, $\gamma = 0.7$, and $\Omega = 10$; and (e) LD/MC/S phase for $\alpha = 0.3$, $\gamma = 0.68$, and $\Omega = 10$. The LK rates are fixed as $\Omega_a = \Omega_d = 0.1$ with $L = 1000$ in all panels.

and disappearance of various standard and mixed phases. Moreover, the nine critical values of the lane-changing rate, beyond which various simple and mixed phases appear and disappear, are identified.

It is seen that the complexity in terms of the number of phases of the phase diagram varies nonmonotonically with the increase in coupling rates. The intermediate values of coupling rates produce complex phase diagrams with fewer phases, indicating that even with a comparatively small change in the entry or exit rates, the path can experience a different phase. Physically, at this state, a small change in the controlling parameters can increase or reduce the traffic on the road or biological paths. The study reveals that higher values of the lane-switching rate lead to the disappearance of the shock phase. Noted that the disappearance of shock has relevance in two aspects as follows. First, it represents the traffic jam on the road or biological path by physical or biological motors, which is a crucial aspect of transportation as it acts like a bottleneck and influences motor mobility. Second, its disappearance at higher values of the coupling rate reveals that fast road switching can reduce traffic jams. It is also crucial to mention that our findings are different from

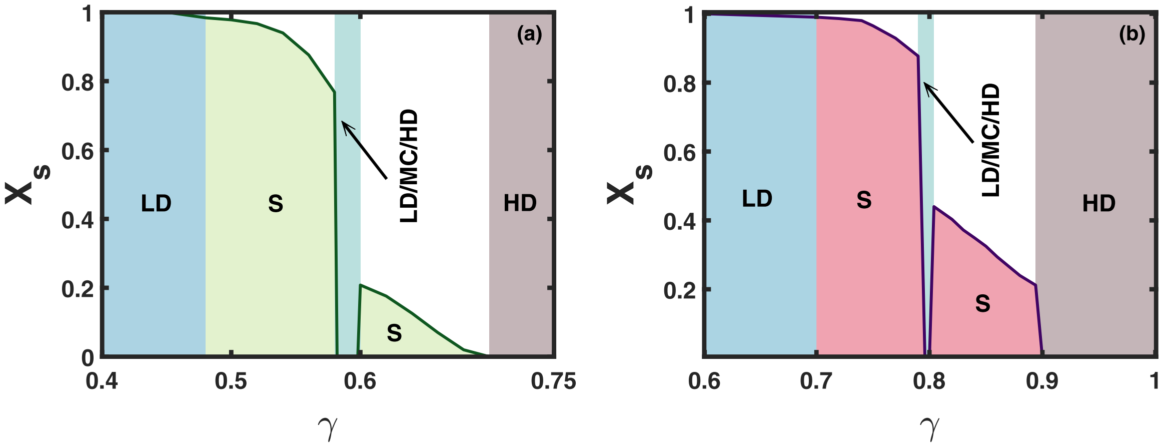

FIG. 7. The corresponding system parameters of shock position of lane A are (a) $\alpha = 0.41$, $\Omega = 1$, (b) $\alpha = 0.2$, $\Omega = 10$ with $\Omega_a = \Omega_d = 0.1$, and lattice size $L = 1000$. We have highlighted the shock region using green (a) and pink (b) in which the value of the shock position is nonzero.

previous studies in terms of observed phases apart from the reported properties. The most strikng feature of the proposed model is the presence of a back-and-forth phase transition which is noticed through an increase in $\gamma = 1 - \beta$ for some constant values of the entry rate α with comparatively smaller values of coupling rates. In this case, we visualized transitions from the LD phase to the S phase and then back to the S phase via some mixed phases due to the interplay between adopted boundary conditions, coupling rules, and Langmuir Kinetics. Based on back-and-forth phase transitions, the proposed study reveals that there can be an optimal value of the entry rate for which the system remains in a nonshock state despite variation in the exit rate, which is important for smooth transportation. Additionally, it is seen that the S phase is partially fragmented by the LD/MC/HD phase in the phase diagram for a comparatively small value of the lane-changing rate. Further, the role of the system size has been analyzed, and it has been proved that there is no finite-size effect on the steady-state features of the proposed system.

The proposed study provides insight into understanding the complex dynamics of some realistic physical stochastic nonequilibrium transport systems under the influence of comparatively more realistic coupling conditions and highlights its nontrivial impact on system dynamics. In this study, we adopt the symmetric coupling conditions, and the more general case of asymmetric coupling situations will be taken up in future models.

APPENDIX A

The model studied in the main text motivated by vehicular traffic does not include the case of simple coupling, which is comparatively more suitable for mimicking the intracellular transport carried out by motor proteins. Here we consider the model with simple coupling conditions after removing extended switching rules presented in the main text to visualize the combined effect of standard coupling and bidirectional particle movement on the phase diagram of the proposed model as follows. Under the simple coupling conditions, the resulting governing equations read as follows.

At bulk sites:

$$\frac{d\rho_A}{dt'} = \frac{\epsilon}{2}\rho_A'' + (2\rho_A - 1)\rho_A' + \Omega_a(1-\rho_A) - \Omega_d\rho_A - \Omega[\rho_A^2(1-\rho_B) - \rho_B^2(1-\rho_A)], \tag{A1}$$

$$\frac{d\rho_B}{dt'} = \frac{\epsilon}{2}\rho_B'' + (1 - 2\rho_B)\rho_B' + \Omega_a(1-\rho_B) - \Omega_d\rho_B + \Omega[\rho_A^2(1-\rho_B) - \rho_B^2(1-\rho_A)]. \tag{A2}$$

The particle density in both lanes at boundaries can be calculated as follows.

At boundary sites:

$$\frac{d\rho_{1,A}}{dt'} = \frac{1}{\epsilon}\alpha(1-\rho_{1,A}) - \frac{1}{\epsilon}\rho_{1,A}(1-\rho_{2,A}), \tag{A3}$$

$$\frac{d\rho_{1,B}}{dt'} = \frac{1}{\epsilon}\rho_{2,B}(1-\rho_{1,B}) - \frac{1}{\epsilon}\beta\rho_{1,B}, \tag{A4}$$

$$\frac{d\rho_{L,A}}{dt'} = \frac{1}{\epsilon}\rho_{L-1,A}(1-\rho_{L,A}) - \frac{1}{\epsilon}\beta\rho_{L,A}, \tag{A5}$$

$$\frac{d\rho_{L,B}}{dt'} = \frac{1}{\epsilon}\alpha(1-\rho_{L,B}) - \frac{1}{\epsilon}\rho_{L,B}(1-\rho_{L-1,B}). \tag{A6}$$

Based on the same mathematical techniques as mentioned in Sec. III, we solve the above systems of equations and obtain the phase diagrams for various values of Ω as shown in Fig. 8. Comparing with Fig. 2, we can make the following observations. It is clear from Fig. 2(a) and Fig. 8(a), for $\Omega = 0.1$, apart from slight shifting in the phase diagram, there is no qualitative or quantitative change in the phase diagram. When we further increase the Ω from 0.1 to 1, we obtain an extra I phase in the absence of extended coupling in a extremely narrow region, while for $\Omega = 10$, apart from shifting in phase boundaries, there is no quantitative change in the phase diagram and the same phases are observed with or without extended coupling [see Figs. 2(b) and 2(c) and Figs. 8(b) and 8(c)]. Further, with $\Omega = 100$, the extended coupling leads to various phases including S, L/MC/S, LD/MC/HD, HD, S/MC/HD, in the phase diagram [see Fig. 2(d)], which are not observed in the phase diagram with simple coupling as shown in Fig. 8(d). For $\Omega = 1000$, the extended coupling results in HD phase

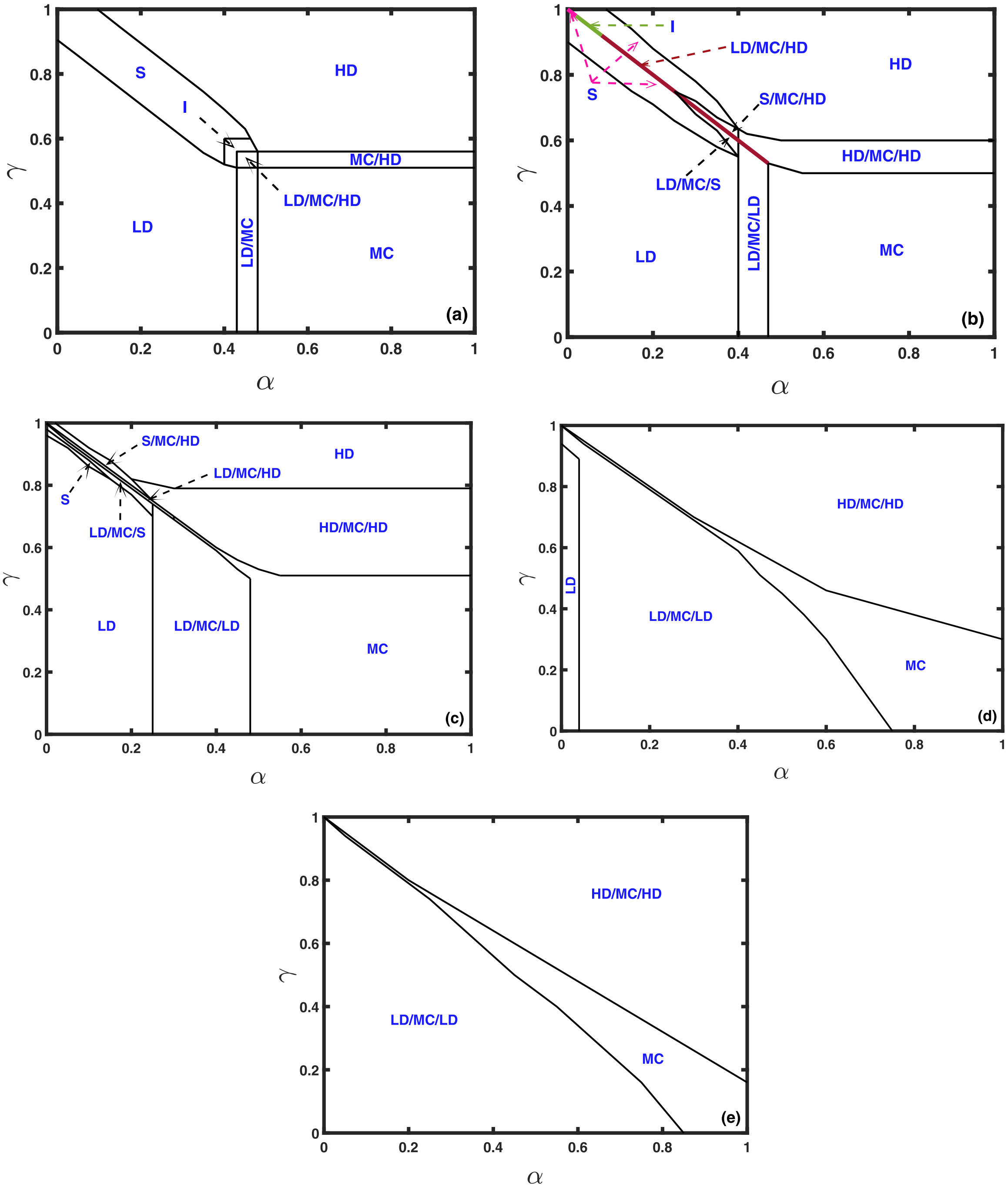

FIG. 8. Phase diagram with simple standard coupling for (a) $\Omega = 0.1$, (b) $\Omega = 1$, (c) $\Omega = 10$, (d) $\Omega = 100$, (e) $\Omega = 1000$ with $\Omega_a = \Omega_d = 0.1$ and $L = 1000$.

in a narrow region in contrast to the simple coupling, which signifies that extended coupling supports particle crowding at roads. Apart from the HD phase, there is no quantitative or significant qualitative change in both phase diagrams. Based on above discussion, we can summarize that the removal of extended coupling rules does not affect system dynamics significantly, and no qualitative changes are observed in the phase diagram with simple coupling. Overall, we obtained the same steady-state phases which were noticed earlier, ignoring the simple coupling. Incorporating simple coupling only leads to shifting in phase boundaries and does not produce any new phase. This motivated us to ignore it in the main text. It also suggests that one can utilize the proposed model and results to understand the dynamics of motor protein transport, since vehicular traffic motivated extended coupling and simple coupling provides almost the same physics.

APPENDIX B

The model studied in main text considers the particles' movement in the opposite direction in lanes, in particular, particles move from left (right) to right (left) in lane A (B).

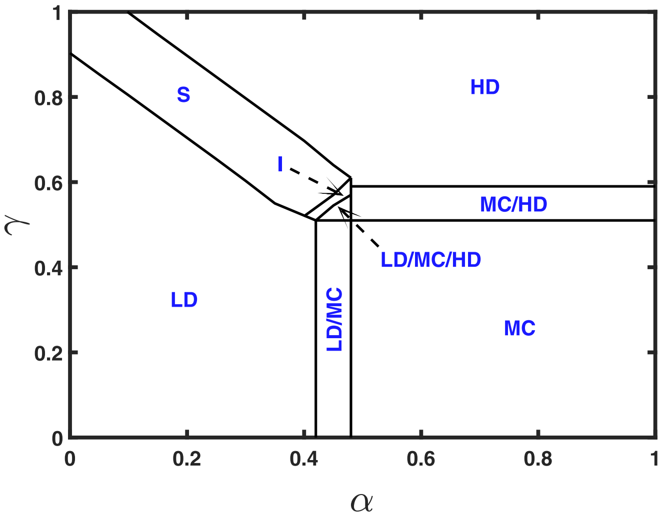

FIG. 9. Phase diagram with unidirectional (left to right) movement in both lanes in the proposed model with $\Omega = 0.1$ and $L = 1000$.

Here we consider the model with unidirectional (right to left) movement in both lanes to scrutinize the combined impact of unidirectional movement and extended lane-changing rules on the system properties of the proposed model as follows. Under the simple coupling conditions, the resulting governing equations read as follows.

At bulk sites:

$$\begin{aligned}\frac{d\rho_A}{dt'} = {} & \frac{\epsilon}{2}\rho_A'' + (2\rho_A - 1)\rho_A' + \Omega_a(1-\rho_A) - \Omega_d\rho_A\\ & - \Omega(1-\rho_A)(1-\rho_B)\big[\rho_A^2(1-\rho_B) - \rho_B^2(1-\rho_A)\big]\\ & - \Omega\epsilon\rho_A'(1-\rho_B)\big[\rho_A(1-\rho_B) + (1-\rho_A)\rho_B^2\big]\\ & + \Omega\epsilon\rho_B'(1-\rho_A)\big[\rho_B(1-\rho_A) + (1-\rho_B)\rho_A^2\big]\\ & + \Omega\epsilon^2\rho_A'\rho_B'(\rho_A - \rho_B) - \Omega\epsilon^2(\rho_A')^2\rho_A(1-\rho_B)^2\\ & + \Omega\epsilon^2(\rho_B')^2\rho_B(1-\rho_A)^2 - \Omega\frac{\epsilon^2}{2}\rho_A''(1-\rho_B)\\ & \times\big[\rho_A(1-2\rho_A)(1-\rho_B) + (1-\rho_A)\rho_B^2\big]\\ & + \Omega\frac{\epsilon^2}{2}\rho_B''(1-\rho_A)\big[\rho_B(1-2\rho_B)(1-\rho_A)\\ & + (1-\rho_B)\rho_A^2\big],\end{aligned} \tag{B1}$$

$$\begin{aligned}\frac{d\rho_B}{dt'} = {} & \frac{\epsilon}{2}\rho_B'' + (2\rho_B - 1)\rho_B' + \Omega_a(1-\rho_B) - \Omega_d\rho_B\\ & + \Omega(1-\rho_A)(1-\rho_B)\big[\rho_A^2(1-\rho_B) - \rho_B^2(1-\rho_A)\big]\\ & + \Omega\epsilon\rho_A'(1-\rho_B)\big[\rho_A(1-\rho_B) + (1-\rho_A)\rho_B^2\big]\\ & - \Omega\epsilon\rho_B'(1-\rho_A)\big[\rho_B(1-\rho_A) + (1-\rho_B)\rho_A^2\big]\\ & - \Omega\epsilon^2\rho_A'\rho_B'(\rho_A - \rho_B) + \Omega\epsilon^2(\rho_A')^2\rho_A(1-\rho_B)^2\\ & - \Omega\epsilon^2(\rho_B')^2\rho_B(1-\rho_A)^2 + \Omega\frac{\epsilon^2}{2}\rho_A''(1-\rho_B)\\ & \times\big[\rho_A(1-2\rho_A)(1-\rho_B) + (1-\rho_A)\rho_B^2\big]\\ & - \Omega\frac{\epsilon^2}{2}\rho_B''(1-\rho_A)\big[\rho_B(1-2\rho_B)(1-\rho_A)\\ & + (1-\rho_B)\rho_A^2\big].\end{aligned} \tag{B2}$$

The resulting particle density at boundaries can be computed as follows.

At boundary sites:

$$\frac{d\rho_{1,A}}{dt'} = \frac{1}{\epsilon}\alpha(1-\rho_{1,A}) - \frac{1}{\epsilon}\rho_{1,A}(1-\rho_{2,A}), \tag{B3}$$

$$\frac{d\rho_{1,B}}{dt'} = \frac{1}{\epsilon}\alpha(1-\rho_{1,B}) - \frac{1}{\epsilon}\rho_{1,B}(1-\rho_{2,B}), \tag{B4}$$

$$\frac{d\rho_{L,A}}{dt'} = \frac{1}{\epsilon}\rho_{L-1,A}(1-\rho_{L,A}) - \frac{1}{\epsilon}\beta\rho_{L,A}, \tag{B5}$$

$$\frac{d\rho_{L,B}}{dt'} = \frac{1}{\epsilon}\rho_{L-1,B}(1-\rho_{L,B}) - \frac{1}{\epsilon}\beta\rho_{L,B}. \tag{B6}$$

Utilizing the same mathematical technique as mentioned in the main text, we solve the above system of equations to calculate the phase diagram, which is displayed in Fig. 9 for $\Omega = 0.1$, which remains the same for any value of $\Omega \in (0, 1000]$ due to symmetric coupling. It is clear from the figure that unidirectional movement in both lanes does not provide any new phase or physics, which motivated us to ignore it in the main text and adopt the bidirectional movement, which is more suitable for various transport systems leading to various steady-state features as discussed in main text. Summarizing, unidirectional movement will lead to the disappearance of many mixed phases and features including bulk-induced phase transitions, back-and-forth transitions, and partial phase division from the system properties. Based on the above observations, we can also conclude that the obtained results arise in the proposed system due to the interplay between bidirectional movement, coupling, and Langmuir kinetics. Further, it is important to note that a two-lane unidirectional coupled system without an extended coupling system has been studied in [36], which does not report phase I, indicating that extended coupling has a significant role on system dynamics and leads to this unique phase in the phase diagram as shown in Fig. 9.

[1] K. Nagel, Phys. Rev. E **53**, 4655 (1996).
[2] K. Nagel, D. E. Wolf, P. Wagner, and P. Simon, Phys. Rev. E **58**, 1425 (1998).
[3] D. Chowdhury, Phys. Scr. **2003**, 13 (2003).
[4] A. John, A. Schadschneider, D. Chowdhury, and K. Nishinari, Swarm Intelligence **2**, 25 (2008).
[5] D. Chowdhury, L. Santen, and A. Schadschneider, Phys. Rep. **329**, 199 (2000).
[6] L. B. Shaw, R. K. P. Zia, and K. H. Lee, Phys. Rev. E **68**, 021910 (2003).
[7] T. Chou and G. Lakatos, Phys. Rev. Lett. **93**, 198101 (2004).
[8] R. Zia, J. Dong, and B. Schmittmann, J. Stat. Phys. **144**, 405 (2011).
[9] S. Klumpp and R. Lipowsky, J. Stat. Phys. **113**, 233 (2003).
[10] B. Widom, J. Viovy, and A. Defontaines, J. Phys. I **1**, 1759 (1991).

[11] C. T. MacDonald, J. H. Gibbs, and A. C. Pipkin, Biopolymers **6**, 1 (1968).
[12] J. Krug, Braz. J. Phys. **30**, 97 (2000).
[13] M. R. Evans, R. Juhász, and L. Santen, Phys. Rev. E **68**, 026117 (2003).
[14] V. Popkov, A. Rákos, R. D. Willmann, A. B. Kolomeisky, and G. M. Schütz, Phys. Rev. E **67**, 066117 (2003).
[15] A. Parmeggiani, T. Franosch, and E. Frey, Phys. Rev. Lett. **90**, 086601 (2003).
[16] R. Jiang, M.-B. Hu, Y.-H. Wu, and Q.-S. Wu, Phys. Rev. E **77**, 041128 (2008).
[17] J. Krug, Phys. Rev. Lett. **67**, 1882 (1991).
[18] V. Popkov, J. Stat. Mech.: Theory Exp. (2007) P07003.
[19] M. R. Evans, D. P. Foster, C. Godrèche, and D. Mukamel, Phys. Rev. Lett. **74**, 208 (1995).
[20] E. Pronina and A. B. Kolomeisky, J. Phys. A: Math. Theor. **40**, 2275 (2007).
[21] A. K. Verma, N. Sharma, and A. K. Gupta, Phys. Rev. E **97**, 022105 (2018).
[22] A. Parmeggiani, T. Franosch, and E. Frey, Phys. Rev. E **70**, 046101 (2004).
[23] S. Muhuri, Europhys. Lett. **101**, 38001 (2013).
[24] A. K. Verma, N. Sharma, and A. K. Gupta, Phys. Rev. E **99**, 032411 (2019).
[25] E. Pronina and A. B. Kolomeisky, J. Phys. A: Math. Gen. **37**, 9907 (2004).
[26] E. Pronina and A. B. Kolomeisky, Physica A **372**, 12 (2006).
[27] K. Tsekouras and A. Kolomeisky, J. Phys. A: Math. Theor. **41**, 465001 (2008).
[28] Q.-H. Shi, R. Jiang, M.-B. Hu, and Q.-S. Wu, J. Stat. Phys. **142**, 616 (2011).
[29] Q.-H. Shi, R. Jiang, M.-B. Hu, and Q.-S. Wu, Phys. Lett. A **376**, 2640 (2012).
[30] B. Saha and S. Mukherji, J. Stat. Mech.: Theory Exp. (2013) P09004.
[31] M. R. Evans, Y. Kafri, K. E. Sugden, and J. Tailleur, J. Stat. Mech.: Theory Exp. (2011) P06009.
[32] V. Yadav, R. Singh, and S. Mukherji, J. Stat. Mech.: Theory Exp. (2012) P04004.
[33] A. K. Gupta and I. Dhiman, Physica A **392**, 6314 (2013).
[34] R. Wang, R. Jiang, M. Liu, J. Liu, and Q.-S. Wu, Int. J. Mod. Phys. C **18**, 1483 (2007).
[35] A. K. Gupta and I. Dhiman, Phys. Rev. E **89**, 022131 (2014).
[36] I. Dhiman and A. K. Gupta, Europhys. Lett. **107**, 20007 (2014).
[37] A. K. Verma, A. K. Gupta, and I. Dhiman, Europhys. Lett. **112**, 30008 (2015).
[38] H. Yamamoto, S. Ichiki, D. Yanagisawa, and K. Nishinari, Phys. Rev. E **105**, 014128 (2022).
[39] R. Jiang, R. Wang, and Q.-S. Wu, Physica A **375**, 247 (2007).
[40] Y.-Q. Wang, R. Jiang, Q.-S. Wu, and H.-Y. Wu, Mod. Phys. Lett. B **28**, 1450123 (2014).
[41] A. K. Gupta, J. Stat. Phys. **162**, 1571 (2016).
[42] A. Schadschneider, D. Chowdhury, and K. Nishinari, *Stochastic Transport in Complex Systems: From Molecules to Vehicles* (Elsevier, Amsterdam, The Netherlands, 2010).
[43] N. Sharma and A. Gupta, J. Stat. Mech.: Theory Exp. (2017) 043211.
[44] S. Ghosh and A. Kunwar, Physica A **570**, 125779 (2021).
[45] A. Jindal, A. K. Verma, and A. K. Gupta, J. Stat. Phys. **182**, 1 (2021).
[46] A. Jindal, A. B. Kolomeisky, and A. K. Gupta, J. Stat. Mech.: Theory Exp. (2020) 113202.
[47] Q.-Y. Hao, R. Jiang, M.-B. Hu, Y. Zhang, C.-Y. Wu, and N. Guo, Phys. Rev. E **100**, 032133 (2019).
[48] A. Jelić, C. Appert-Rolland, and L. Santen, Europhys. Lett. **98**, 40009 (2012).
[49] Xiaoyu Song Xiao, X. Chen, and Y. Liu, Russ. J. Phys. Chem. B **14**, 929 (2020).
[50] N. Sharma, A. K. Verma, and A. K. Gupta, Phys. Lett. A **382**, 1383 (2018).
[51] S. Mukherji and V. Mishra, Phys. Rev. E **74**, 011116 (2006).
[52] A. K. Verma and A. K. Gupta, J. Stat. Mech.: Theory Exp. (2019) 103210.